

Article

Characteristic Analysis of Electromagnetic Force in a High-Power Wireless Power Transfer System

Xian Zhang ¹, Xuejing Ni ^{1,*} , Bin Wei ², Songcen Wang ² and Qingxin Yang ¹

¹ Tianjin Key Laboratory of Advanced Electrical Engineering and Energy Technology, Tianjin Polytechnic University, Tianjin 300387, China; zxshow1983@163.com (X.Z.); qxyang@tjpu.edu.cn (Q.Y.)

² China Electric Power Research Institute, Beijing 100085, China; Weibin@epri.sgcc.com.cn (B.W.); wangsongcen@epri.sgcc.com.cn (S.W.)

* Correspondence: nxj838435084@163.com; Tel.: +86-133-5172-7553

Received: 15 October 2018; Accepted: 6 November 2018; Published: 8 November 2018



Abstract: In order to explore the influence of the electromagnetic force (EMF) on the coupling mechanism in a high-power wireless power transfer (WPT) system, the characteristics of the EMF are investigated by theoretical calculation and simulation. The expressions of the EMF on the WPT structure with magnetic shielding are derived in time domain and frequency domain, respectively. The EMF is divided into Lorentz force and Kelvin force. The distribution and changing regularity of the EMF on the coil and the magnetic shield under different exciting currents are solved by the finite element model, and the harmonic of the EMF is analyzed in detail. The results show that the coil is subjected to the EMF in both radial and axial directions. The EMF on the magnetic shield is opposite to the EMF on the coil, and the force between the transmitting coil and the receiving coil is repulsive. The frequency of the EMF is twice that of the system resonant frequency. An experimental prototype is built to prove the correctness of the predicted characteristics. It is shown that the EMF should be carefully considered in the application of high-power WPT systems.

Keywords: electromagnetic force (EMF); wireless power transfer (WPT); high-power; coupling mechanism; high-frequency current

1. Introduction

Wireless power transfer (WPT), because of its convenience, safety, flexibility, and some other advantages, has been extensively used in many fields such as mobile phones, biomedicines, smart homes, and communication [1–4]. In recent years, with the gradual growth of the global energy revolution, WPT technology has been progressively developing to high-power applications from the kilowatt to the megawatt power level. As an emerging technology, wireless charging for electric vehicles could solve the drawbacks of low battery capacity and time-consuming and labor-intensive plug-in charging [5–7]. Considering the fact that high-speed train pantograph is easy to wear and produce electric arc, which leads to unreliable power supply, WPT used in high-speed rail is also a hot research topic [8,9]. Moreover, inductive power transfer for marine mechanisms such as ships could reduce the impact of extreme weather at sea and of limited berthing time [10].

However, the coupling mechanism in WPT systems, owing to the existence of inductive current and time-varying electromagnetic fields, is inevitably affected by the electromagnetic force (EMF). With the increase of transmission power, the excitation current and space-coupling magnetic field will be increased. Thus, the EMF in high-power WPT systems has not to be ignored.

EMF has been researched by several methods in numerous fields [11]. An improved superposition method was proposed to predict the unbalanced magnetic force of permanent magnet machines.

In reference [12], the cross-frequency of EMF in the induction heating application of a linear induction motor, which could improve the stability of the system, was investigated.

For WPT systems, a study [13] proposed a type of micro-robot, which could transmit energy through a magnetic field, and the EMF on the receiving coil also provide a driving force to the robot. To precisely control turning and tracing of the robot, a study [14] floated the receiving coil on water, and the characteristics of EMF were obtained by calculating the drift velocity of the coil. The authors assumed that the magnetic field was perpendicular to the receiving coil and only generated a tangential force on the coil.

However, the EMF of a high-power WPT system has rarely been analyzed. In practical applications, the magnetic field is alternating, which will generate EMF in various directions, and most of the EMF has negative effects rather than being a driving force [15,16]. Generally, EMF is the main inducer of a continuous periodic vibration causing the braking of the mechanism. Under the long-term action of the EMF, service life, security, and reliability of WPT system will deteriorate. In addition, the EMF also produces noise pollution in the surrounding environment [17]. The characteristics of EMF on a ferromagnetic material in a WPT system were analyzed in reference [18], which only considered the receiver and did not obtain exact conclusions on the effects of the EMF on the WPT system.

In this paper, on the basis of the high-power wireless power transfer system, detailed characteristics of the EMF on the coupling mechanism with magnetic shielding in WPT are revealed. The paper is organized as follows. Section 2 will classify the EMF in a WPT system on the basis of the traditional Korteweg–Helmholtz force density method of EMF. In Section 3, this paper will deduce the analytic expressions of the EMF on the coupling mechanism of a high-power WPT system and obtain the theoretical distribution characteristics and frequency characteristics of the EMF. At the same time, the magnitude of the EMF will be solved by means of the finite element method, and the correctness of the theoretical analytic results will also be verified by the simulation. In Section 4, an experimental prototype will be built to verify the correctness of the characteristics. Further, the change regulation of the EMF will be discussed. Section 5 will draw conclusions about this paper.

2. Classification and Model of EMF in WPT

The structure of the commonly used coupling mechanism in a WPT system is presented in Figure 1. I_1 is the exciting current of the transmitting coil (Tx-coil), generating magnetic flux density B in the coupling domain. The magnetic field produces inductive current I_2 in the receiving coil (Rx-coil), which is rectified and inverted to supply load, delivering energy without any electrical connection. Considering the location in which the WPT system is installed in high-power applications, a square coil has been used to improve space utilization. The magnetic shielding is ferromagnetic material, added to optimize the distribution of the magnetic field and improve the transmission efficiency in the WPT system.

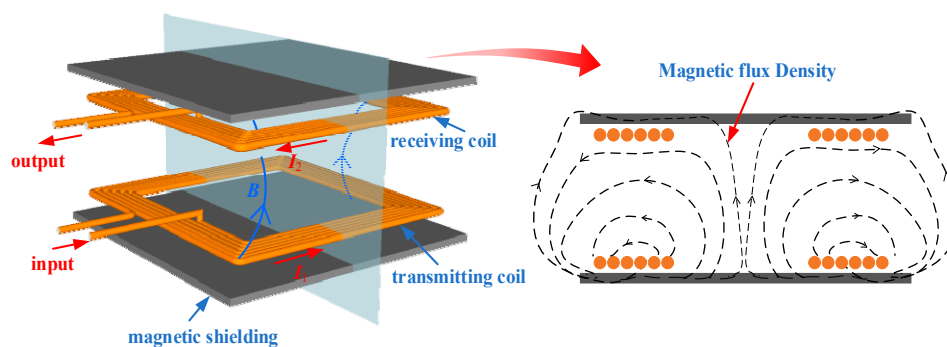


Figure 1. Schematic and two-dimensional section of the wireless power transfer (WPT) system.

The exciting current of the WPT system is sinusoidal and alternating, thus the displacement current can be ignored, and the magnetic field generated by the coupling mechanism can be

equivalent to the magnetoquasistatic field. Meanwhile, because the materials of WPT system are linear and incompressible, the Korteweg–Helmholtz force density method [15] is used to investigate the characteristics of the EMF coupling coils and magnetic shielding materials, neglecting magnetostriction. The EMF density f on the unit volume of the mechanism is expressed as:

$$f = J \times B - \frac{1}{2} H \cdot H \nabla \mu = f_J + f_M \quad (1)$$

where J is the current density in the coils, B refers to the magnetic flux density, H denotes the magnetic field intensity, μ is the permeability of the shielding. The relationship between B and H of magnetically linear materials is $B = \mu_0(H + M) = \mu H$.

It can be seen that the EMF in the WPT system consists of Lorentz force f_J and Kelvin force f_M . f_M is produced by the interaction between the magnetic field and the magnetizing current. The material of coupling coils in WPT is copper, whose permeability almost nears 1, so the coils cannot be magnetized but only subjected to Lorentz force f_J . Generally, magnetic shielding materials in WPT are linear soft magnetic materials, the conductivity of which is very small, and the eddy current of which can be ignored. Thus, Kelvin force f_M is just acting on the magnetic shielding.

In order to study the characteristics of the EMF on the WPT mechanism, a finite element analysis model is built according to Figure 1. The important parameters of the coupling mechanism are given in Table 1. In order to reduce the alternating current (AC) resistance loss of the coils in the high-power system, a 10.89 kHz frequency is adopted. The transmission distance is set to 20 cm according to the actual electric vehicle or high-speed rail chassis height. The exciting current is adjustable for simulating the states of different output powers, with an initial value of 171.8 A.

Table 1. Parameters of the electromagnetic force (EMF) model.

Parameters	Value
Resonant frequency	10.89 kHz
Exciting current amplitude	171.8 A
Wire radius	0.4 cm
Ferrite relative permeability	2500
Transmission distance	20 cm

3. Electromagnetic Force Calculation and Analysis

3.1. Current Calculation in WPT with Magnetic Shielding

Figure 2 illustrates the most basic series–series compensated topology of the WPT system with magnetic shielding, in which r_1 is the sum of the resistances of the source U_s and the transmitting coil, r_2 is the sum of the resistances of the receiving coil and the load, and L_1 and L_2 represent the transmitting coil and the receiving coil, respectively. M is the mutual inductance of the coils, and Δr_1 , Δr_2 , ΔM are the additional resistances and mutual-inductance caused by the magnetic shielding, respectively. Because the resonant capacitors, C_1 and C_2 , matched the inductance, making the system work at resonance frequency ω , the additional inductance is ignored. Equation (2) shows Kirchhoff's voltage equation of the system.

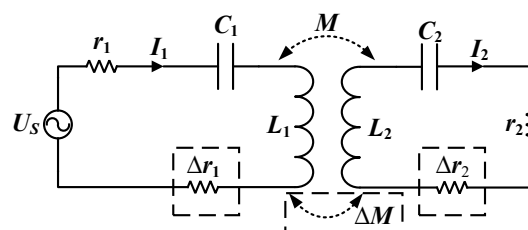


Figure 2. Series-series compensated topology of the WPT system with magnetic shielding.

$$\begin{bmatrix} U_S \\ 0 \end{bmatrix} = \begin{bmatrix} r_1 + \Delta r_1 & -j\omega(M + \Delta M) \\ -j\omega(M + \Delta M) & r_2 + \Delta r_2 \end{bmatrix} \cdot \begin{bmatrix} I_1 \\ I_2 \end{bmatrix} \quad (2)$$

The exciting current I_1 and inductive current I_2 can be obtained, as shown in Equation (3). It can be shown that the amplitude of the currents is related to the increments of the resistances and mutual inductance, which depend on the shape and location of the magnetic shielding. Figure 3 shows the currents of the coupling coils in the simulation.

$$\begin{cases} I_1 = \frac{(r_2 + \Delta r_2) \cdot U_S}{(r_1 + \Delta r_1)(r_2 + \Delta r_2) + \omega^2(M + \Delta M)^2} \\ I_2 = \frac{j\omega(M + \Delta M)}{r_2 + \Delta r_2} I_1 \end{cases} \quad (3)$$

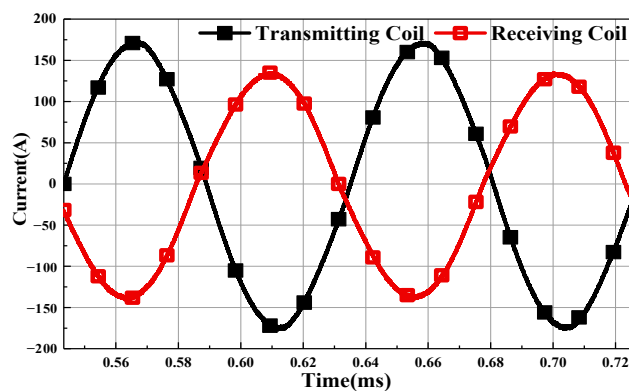


Figure 3. Waveforms of the resonant currents in the analysis model.

3.2. Magnetic Field Calculation in WPT

The magnetic field in WPT is regarded as a two-dimensional axisymmetric field, as shown in Figure 4. Firstly, only considering the coils in the system, the magnetic flux density B at any position in the coupling domain is generated by the exciting current J_1 and the inductive current J_2 together:

$$B = \frac{\mu_0 N}{4\pi} \sum_{i=1,2} \int_V \frac{J_i \times e_{R_i}}{R_i^2} dV = -\frac{\mu_0 N}{4\pi} \sum_{i=1,2} J_i \times \int_V \nabla \frac{1}{R_i} dV \quad (4)$$

where dV is the unit volume of the coils, R is the distance from field point to dV , N is the number of coil turns.

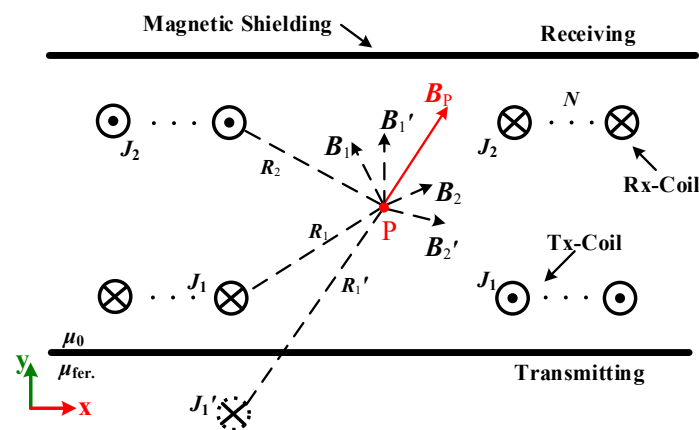


Figure 4. Diagrammatic sketch of magnetic flux density and EMF.

However, magnetic shielding materials, such as Mn–Zn ferrite and other materials with high permeability, are often used in practical applications. Since the coil is closely attached to the magnetic shielding, the magnetic field in the coupler can be equivalent to a semi-infinite field, calculated by the image method. Normally, the magnetic shielding in a WPT system is unsaturated, and the magnetic flux lines can be completely closed through the magnetic shielding, thus the thickness of the magnetic shielding can be ignored.

Because the permeability of the magnetic shielding $\mu_{fer.}$ is much larger than μ_0 , the mirror current J_1' is similar to J_1 with the same direction and size and can be derived from Equation (5)

$$J_1' = \frac{\mu_{fer.} - \mu_0}{\mu_{fer.} + \mu_0} J_1 \approx J_1 \tag{5}$$

The magnetic flux density at point P is expressed in Equation (6). Figure 5 shows the distribution of B in the coupling domain.

$$\mathbf{B} = -\frac{\mu_0 N}{4\pi} \sum_{i=1,2} J_i \times \int_V \left(\nabla \frac{1}{R_i} + \nabla \frac{1}{R_i'} \right) dV = B_x e_x + B_y e_y \tag{6}$$

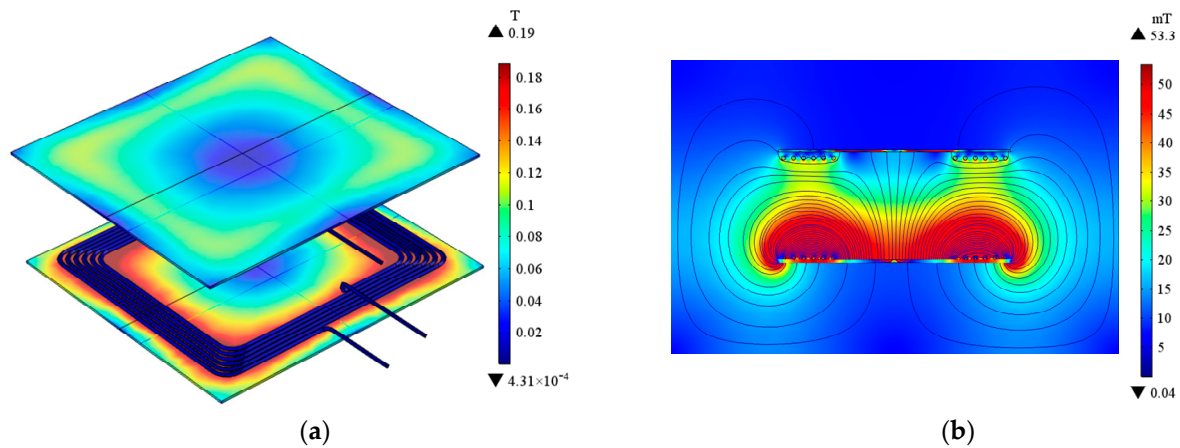


Figure 5. Distribution of magnetic flux density of the coupler in (a) 3D, (b) 2D.

3.3. Calculation of the Electromagnetic Force on the Coils

The EMF density exerted on the unit volume of the coils can be obtained from:

$$\mathbf{f}_J = \mathbf{J} \times \mathbf{B} = f_{Jx} e_x + f_{Jy} e_y \propto (1 + k)^i J_1^2 \tag{7}$$

$$\begin{cases} f_{Jx} = -JB_y \\ f_{Jy} = JB_x \end{cases} \tag{8}$$

where f_{Jx} and f_{Jy} are the x - and y -axis components of the Lorentz force on the coils, respectively, and $k = \omega(M + \Delta M) / (r_2 + \Delta r_2)$ is the ratio of the currents in the coils. Thus, we can obtain the EMF on the coils by the volume integral of the force density f_J :

$$\mathbf{F}_J = \int_V \mathbf{f}_J dV \tag{9}$$

The EMF is of the unidirectional pulsating type because it is proportional to the current squared. Taking a one-turn transmitting coil as an example, the direction of the EMF can be determined by the left-hand rule, as shown in Figure 6. It can be seen that two tangential forces on the same section of the one-turn coil, F_{Jxa} and F_{Jxb} , are equal in magnitude and opposite in direction. Since the coils in WPT

can be regarded as closed coils, the EMF on the coils in the x -axis cancel each other out [14]. Therefore, for the whole closed coil, the EMF in the x direction is zero. However, the long-term action of the force will make the coil expand or contract gradually, which has a negative influence on the shape and life of the coil. The normal components on the one-turn coil, F_{Jya} and F_{Jyb} , are a constant throughout in the same direction. The variation of the force with time is shown in Figure 7.

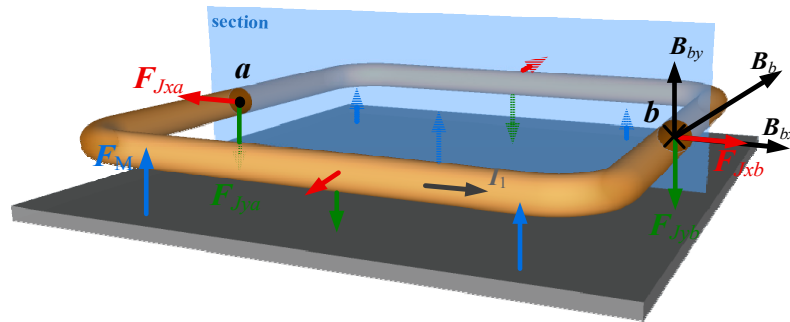


Figure 6. Schematic of the EMF on a one-turn transmitting coil in a 2D section.

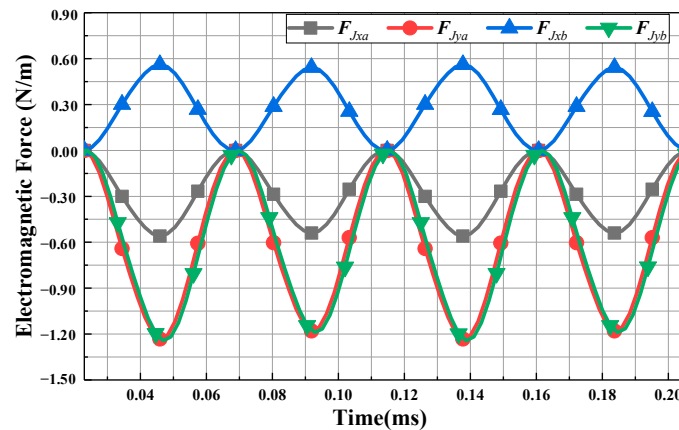


Figure 7. EMF on a one-turn transmitting coil in a 2D section.

For the whole series-series compensated coupling multi-turn coils, the EMF acting on the coils is the resultant force of F_J on each one-turn coil. However, because the magnetic field is not uniformly distributed in the coupling space, Figure 8 shows the EMF on each turn of multi-turn coils. It can be seen that F_{Jy} on the middle turn is the largest, and F_{Jy} on the transmitting coil is always downward. However, the values of F_{Jx} on the side turns are larger, and the directions are inconsistent. By integrating the results of Figure 8, the EMF of the whole multi-turn coils can be obtained, as shown in Figure 9.

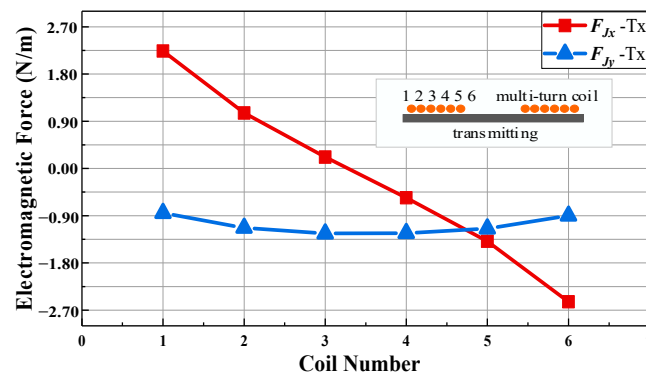


Figure 8. EMF on each turn of multi-turn transmitting coils.

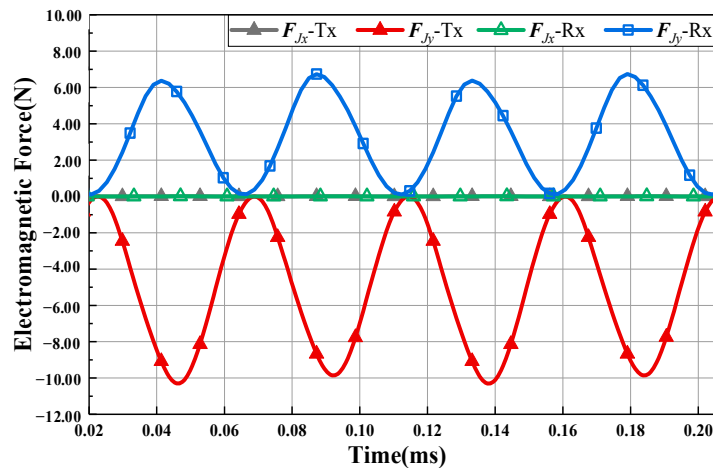


Figure 9. The resultant EMF on multi-turn coils.

As a result of the cancellation of F_{Jx} on each turn of the coil, F_{Jx} on multi-coils is still zero. However, expansion or compression in the radial direction of the coils still exist, which will cause deformation and fracture of the coils. In the commonest WPT systems, the amplitude of the inductive current J_2 is less than that of the exciting current J_1 , $k < 1$, and the magnetic field near the Rx-coil is lower than that near the Tx-coil. Thus, F_{Jy} on the Rx-coil is less than F_{Jy} on the Tx-coil. F_{Jy-Tx} and F_{Jy-Rx} are -10.3 N and 6.2 N, respectively, which is consistent with the rule of Equation (9). Note that, considered from the direction of the magnetic field, F_{Jy-Tx} is vertically downward, and F_{Jy-Rx} is vertically upward, so their directions are opposite, that is, there is a repulsive force between the transmitting and the receiving coil.

3.4. Electromagnetic Force on Magnetic Shielding Calculation

From Maxwell theory, the EMF is delivered through the space medium. So, f_M from Equation (1) could be calculated by the Maxwell stress method. The EMF acting on the unit surface area of magnetic shielding is

$$\mathbf{p} = \frac{1}{\mu_0}(\mathbf{n} \cdot \mathbf{B})\mathbf{B} - \frac{1}{2\mu_0}B^2\mathbf{n} \quad (10)$$

$$\begin{cases} p_x = \frac{1}{2\mu_0}B_x B_y \\ p_y = \frac{1}{2\mu_0}(B_y^2 - B_x^2) \end{cases} \quad (11)$$

where \mathbf{p} is the Maxwell tensor, and \mathbf{n} is the normal unit vector of the surface.

Kelvin force f_M is caused by the change in the magnetic permeability μ at the interface of the ferromagnetic materials and the direction of f_M is from large permeability to low permeability. In a WPT system, the permeability of magnetic shielding μ_{fer} is about 2500–3500 times μ_0 , thus \mathbf{B} is perpendicular to the magnetic shielding surface. The EMF on the magnetic shielding is shown in Equation (12), and its direction is also perpendicular to the surface.

$$F_M = \int_S \mathbf{p} dS = \int_S \frac{1}{2\mu_0} B^2 \mathbf{n} dS \propto J_i^2 \quad (12)$$

From Equation (12), the amplitude of F_M only depends on the strength of the magnetic field and the shape of the shielding. Since most of the magnetic flux lines go through the shielding, the amplitude of F_M is larger than that of F_J . Figure 10 shows that F_M on the transmitting shield is 12.28 N, while F_{Jy-Tx} is only -8.2 N. The direction of F_M should point to the source of the magnetic field, thus F_M points to the coil: in other words, the directions of F_M and F_J on the transmitting mechanism or the receiving mechanism are opposite.

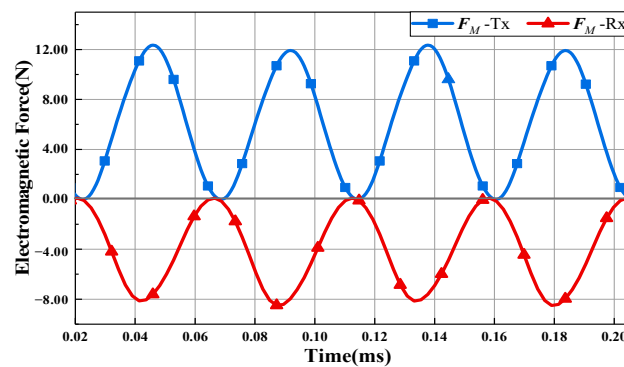


Figure 10. EMF on the magnetic shielding of the WPT system. Relative permeability μ is 2500.

3.5. Electromagnetic Force Analysis in Frequency

In the time-varying electromagnetic field with resonance angular frequency ω generated by the WPT system, when J and B are considered as standard sine functions, expressed by

$$\begin{cases} J(t) = \sqrt{2}J \sin(\omega t + \varphi_J) \\ B(t) = \sqrt{2}B \sin(\omega t + \varphi_B) \end{cases} \quad (13)$$

the EMF density f_j exerted on coils and the surface tensor p of magnetic shielding could be obtained as follows:

$$\begin{cases} f_{j_i} \propto J_i^2(t) + \prod_{i=1,2} J_i(t) = 2J_i^2 \sin^2(\omega t + \varphi_{J_i}) + 2 \prod_{i=1,2} J_i \sin(\omega t + \varphi_{J_i}) \\ = [J_i^2 + J_1 J_2 \cos(\varphi_{J_1} - \varphi_{J_2})] - \begin{bmatrix} J_i^2 \cos(2\omega t + 2\varphi_i) + \\ J_1 J_2 \cos(2\omega t + \varphi_{J_1} + \varphi_{J_2}) \end{bmatrix} \\ p = \frac{1}{2\mu_0} B(t)^2 n = \left[\frac{1}{\mu_0} B^2 - \frac{1}{\mu_0} B^2 \cos(2\omega t + 2\varphi_B) \right] n \end{cases} \quad (14)$$

It can be seen that both Lorentz force and Kelvin force have a steady component and a periodic component. The amplitude of f_{j_i} and p relate to the phases of the currents, φ_{J_1} and φ_{J_2} . As the WPT system resonates at the operating frequency ω , the phase difference of the currents is about 90 degrees [19]. From Equation (14), because $J_1 J_1 > J_1 J_2 > J_2 J_2$, the directions of the periodic components of f_{j_1} and f_{j_2} are opposite, which conforms to the conclusion of Section 3.3. Comparing Figures 9 and 10, the directions of the steady components of F_j and F_M are opposite, which means that they can cancel each other out by using appropriate structure parameters of the system, while the periodic components cannot cancel each other out because of the phase difference between F_j and F_M . Thus, the influence of the EMF on the WPT system is mainly caused by the periodic components.

Note that, in Equation (14), the frequency of the periodic force is 21.78 kHz, which is twice that of the system. However, the exciting current often has harmonic components in the actual case, expressed as

$$J(t) = J_0 + \sum_{n=1}^{\infty} \sqrt{2} J_n \sin(n\omega t + \varphi_{J_n}) \quad (15)$$

where J_0 is the steady component of J , and J_n and φ_{J_n} are the effective value and phase of the harmonic components, respectively. Referring to (14), when the currents have harmonic components, the EMF is represented by the interaction of each harmonic. Figure 11 shows that the currents in the WPT mainly contain fundamental and odd harmonics, such as third harmonic and fifth harmonic, and the fundamental is the biggest component. Thus, the main frequencies of the EMF harmonic components are 21.78 kHz, 43.56 kHz, 65.34 kHz, as shown in Figure 11. Meanwhile, the component of the EMF at 21.78 kHz frequency is still dominant.

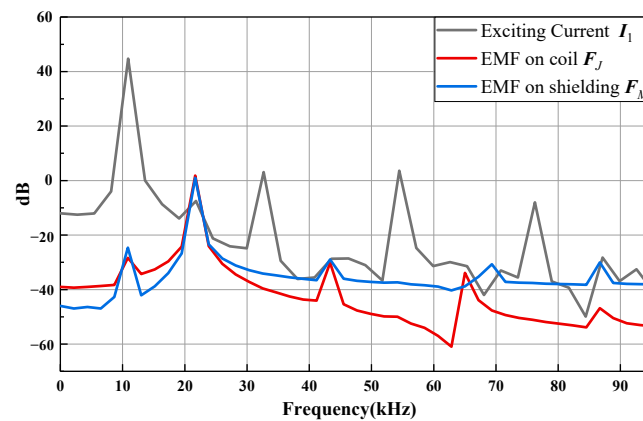


Figure 11. Frequency spectrums of the current and EMF on the coil and the magnetic shielding.

4. Experiment and Discussion

4.1. Experiment Verification

In this section, an isometric experimental prototype is built to verify the characteristics of the EMF described in the former sections, as shown in Figure 12a. In order to simulate the high-power wireless supply with different powers, an adjustable high-frequency current was supplied to the transmitting coil.

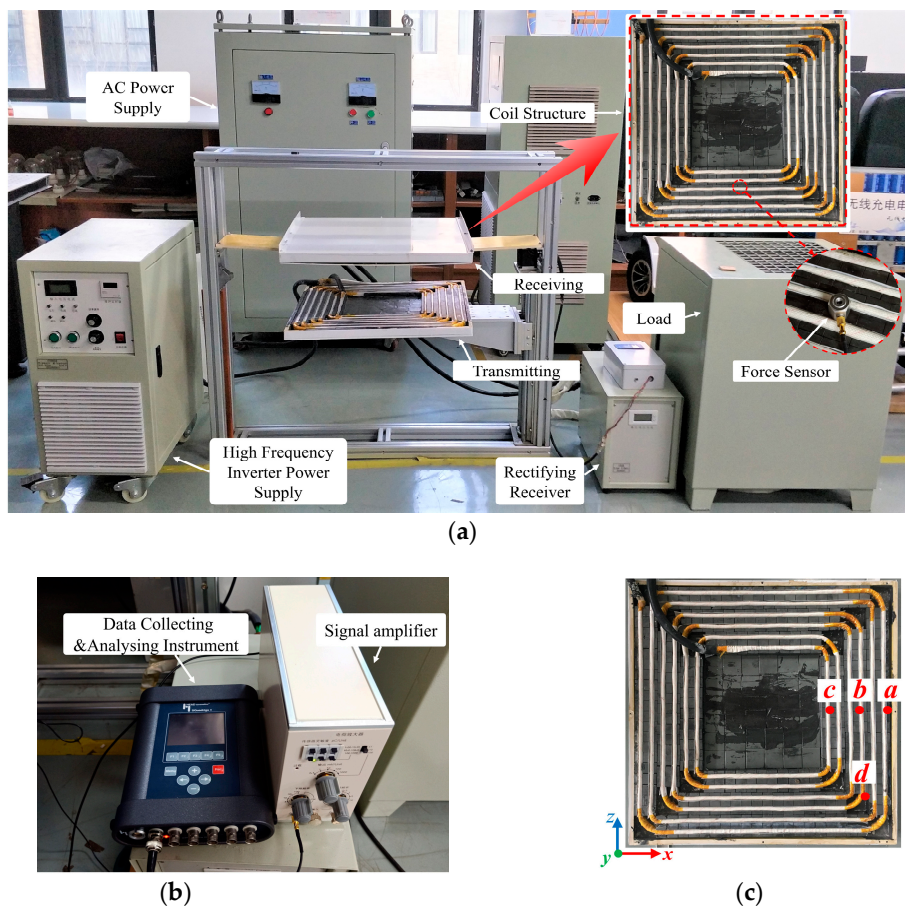


Figure 12. Prototype of the high-power WPT system and data acquisition device. (a) Prototype of high-power WPT system, (b) acquisition system, (c) measuring points on the transmitting coil.

Because the common vibration acceleration sensor does not allow to meet the requirements of the resonant frequency of the WPT system, we have used a high-frequency dynamic force sensor to measure the EMF on the different positions of the coupling mechanism. Because of the complexity of the EMF and of its structure, only the resultant forces of F_J and F_M on the transmitting or receiving coils could be measured. The measuring points are indicated in Figure 12c. Considering that the current density at the corner of the square coil is nonuniform, the point d was selected as the measuring point. On the basis of the interpretations above, the EMF values in the xz plane will cancel each other out, and the EMF on the whole mechanism will be finally reflected in the y direction; therefore, the following measure mainly focuses on the EMF in the y -axis of the coupling mechanism.

When the amplitude of the exciting current was set to 171 A and 215 A respectively, the measured resultant values of EMF on the transmitting coil were determined and are shown in Figure 13. The values only represent the local EMF at the position of the sensor, and the EMF on the whole structure should be obtained by integration. Since the accurate measurement of the EMF is quite hard, it can be considered that both magnitude and tendency are in good agreement. From Figure 13, the EMF will increase 2–4 times rapidly when the current increases 1.26 times. It is obvious that the growth rate of the EMF is much larger than that of the current, because the increase is due to the combination of the current and the magnetic field. The position on the whole coupling mechanism with the largest EMF was point b , which is the middle turn of the coil.

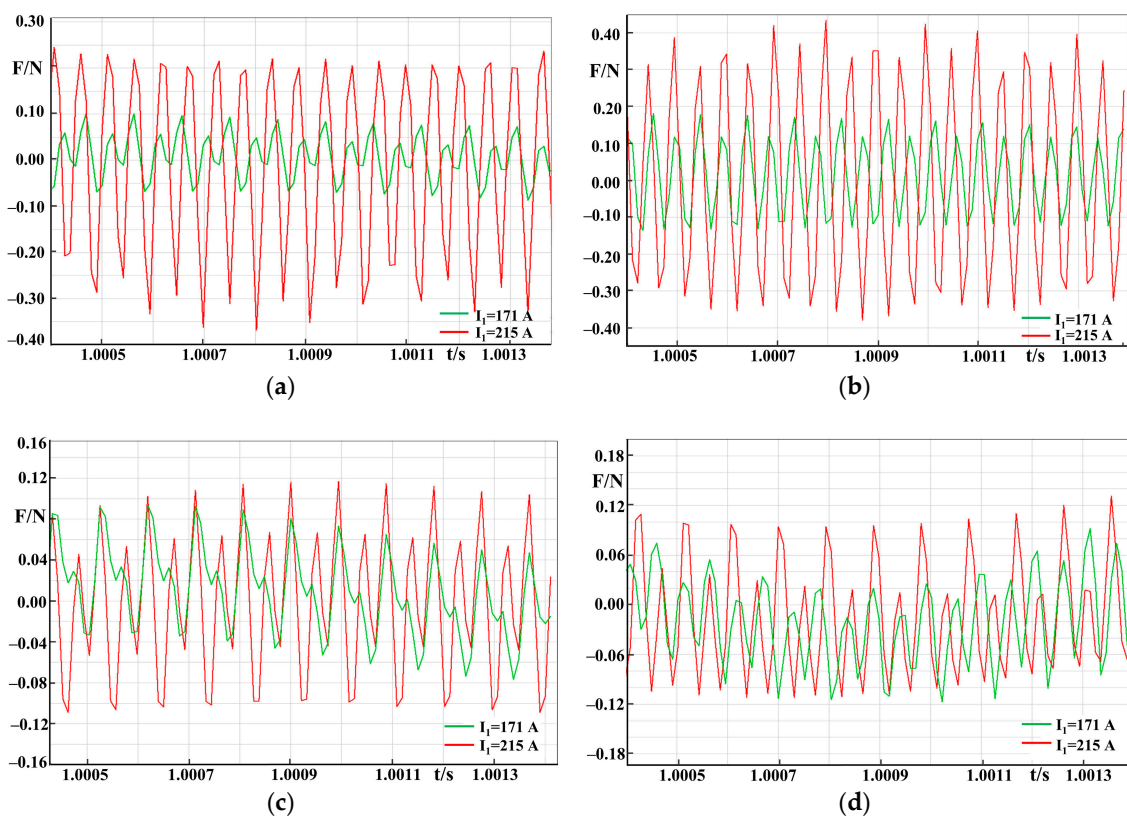


Figure 13. EMF on the measuring points of the transmitting coil. (a) Point a, (b) point b, (c) point c, (d) point d.

Because the structure of the coupling mechanism is symmetrical, the distribution and variation of the EMF on the receiving coil are the same as those of the transmitting coil. Figure 14 shows the amplitude of the EMF on the receiving coil with different current. It can be seen that the EMF on the receiving coil is less than that of transmitting coil, demonstrating the consistency of the simulation experiment.

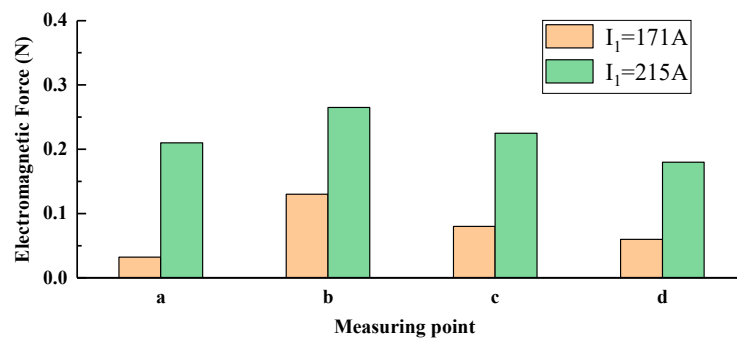


Figure 14. EMF on the measuring points of the receiving coil.

Figure 13 also reveals that there are both a steady component and a periodic component in the EMF, and the steady component of the resultant force is smaller, as a result of F_J and F_M partially canceling each other out. Figures 15 and 16 display the frequency spectrums of the currents and the EMF on the different measuring points. It can be seen that the major frequency of the EMF was 21.78 kHz, which is twice the system resonant frequency. The frequency of the EMF mainly contains the fundamental and the even component, which once again verifies the correctness of the theory.

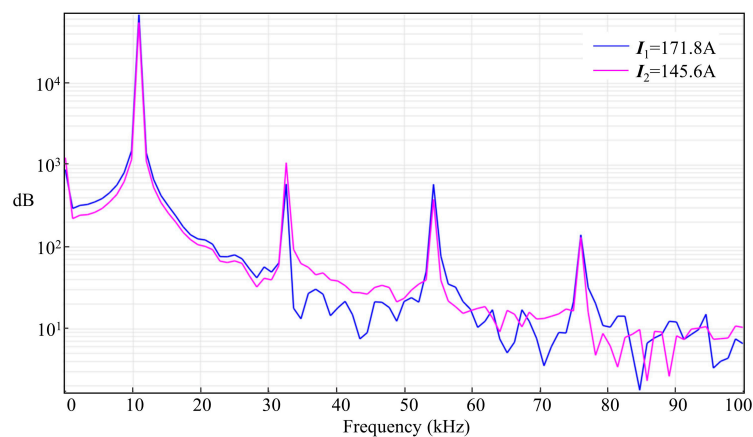


Figure 15. Frequency spectrum of the exciting and inductive currents.

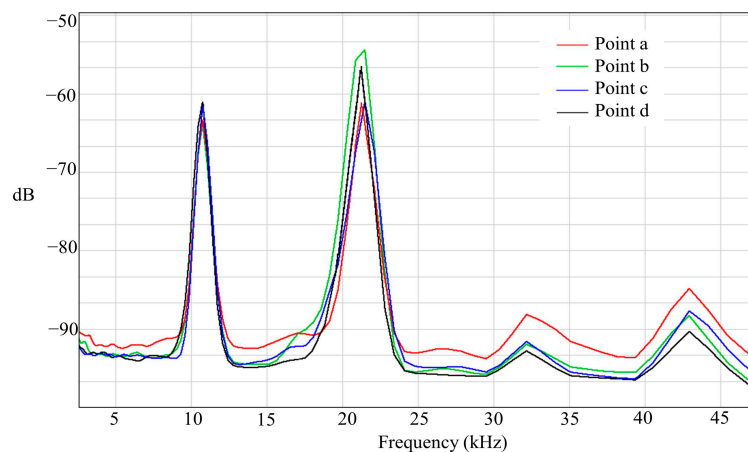


Figure 16. Frequency spectrum of the EMF on the measuring points.

4.2. Discussions

The distribution and direction of the EMF were described in the previous sections, but the amplitude of the EMF depends on the current, the magnetic field, and the structure of the coupling

mechanism. With the increase of wireless transmission power in recent years, with the charging power of an electric vehicle being 7 kW and the traction power of a high-speed train being about 8.8 MW, it is difficult to meet the power demands of this kind of high-power systems by adopting a 6-turn coil. We have calculated the EMF when using coils with a higher number of turns in the basis of the previous model. The exciting current still set to 171 A, the EMF in the y-axis on the 10-turn coil and the 15-turn coil were 18.88 N and 24.85 N, respectively, while the EMF on the 6-turn coil was only 10.3 N. It can be seen that the EMF will increase rapidly with the increase of the number of coil turns, and, as the current continues to increase, the EMF will keep enlarging. Meanwhile, when a sudden short circuit or open circuit occurs on the receiving coil, an enormous transient EMF will be generated, which will impact the stability of the structure. Therefore, the EMF cannot be ignored in high-power applications. However, using the laws mentioned above, a reasonable design of the coil and a magnetic shielding can reduce the steady component of the EMF to enhance the reliability of high-power WPT systems.

5. Conclusions

In this paper, the characteristics of the EMF in a high-power WPT system were studied by theoretical analysis and simulation. The coils will keep expanding or compressing in the radial direction and repel each other in the axial direction because of the effect of the EMF. The EMF on a multi-turn coil is represented by the superposition of different forces on each turn, and the EMF on the coils and the magnetic shielding are in opposite directions. By frequency-field analysis, the resultant EMF on the coupling mechanism contains a steady component and a periodic component, and the periodic component mainly contains the fundamental and the even frequency. The amplitude of the EMF can be solved by the finite element method, which will increase rapidly with the increase of the current and the magnetic field. When the exciting current is 171A, the EMF values on the 6-turn, 10-turn, and 15-turn coil are 10.3 N, 18.88 N and 24.85 N, respectively. In future work, we will propose a smooth method to reduce the EMF on the coupling mechanism of the high-power WPT system and explore the effect of EMF on a dynamic WPT system and the EMF on the external metal foreign body to improve the stability and reliability of WPT systems.

Author Contributions: The paper was written by X.Z. and X.N. and revised by B.W. and S.W. The project was conceived, planned, and supervised by Q.Y. All authors have contributed to the editing and proofreading of this paper.

Funding: This research was funded by the National Natural Science Foundation of China under Grant 51677132 and Grant 51477117, the Fostering Program for Innovation Teams of Tianjin Higher Education Institutions under Grant TD13-5040, and the Program for Science and Technology of State Grid Corporation of China under Grant DG71-17-018.

Conflicts of Interest: The authors declare no conflict of interest.

References

1. Liu, Y.; Li, B.; Huang, M.; Chen, Z.; Zhang, X. An overview of regulation topologies in resonant wireless power transfer systems for consumer electronics or bio-implants. *Energies* **2018**, *11*, 1737. [[CrossRef](#)]
2. Liu, G.; Zhang, B.; Xiao, W.; Qiu, D.; Chen, Y.; Guan, J. Omnidirectional wireless power transfer system based on rotary transmitting coil for household appliances. *Energies* **2018**, *11*, 878.
3. Zhang, Z.; Pang, H.; Georgiadis, A.; Cecati, C. Wireless power transfer—An overview. *IEEE Trans. Ind. Electron.* **2019**, *66*, 1044–1058. [[CrossRef](#)]
4. Bi, S.; Zeng, Y.; Zhang, R. Wireless powered communication networks: An overview. *IEEE Wirel. Commun.* **2016**, *23*, 10–18. [[CrossRef](#)]
5. Zhu, C.; Jiang, J.; Song, K.; Zhang, Q. Research progress of key technologies for dynamic wireless charging vehicle. *Autom. Electr. Power Syst.* **2017**, *41*, 60–65. (In Chinese)
6. Elnail, K.; Huang, X.; Chen, X.; Tan, L.; Xu, H. Core structure and electromagnetic field evaluation in WPT systems for charging electric vehicles. *Energies* **2018**, *11*, 1734. [[CrossRef](#)]

7. Yang, Y.; El Baghdadi, M.; Lan, Y.; Benomar, Y.; Van Mierlo, J.; Hegazy, O. Design methodology, modeling, and comparative study of wireless power transfer systems for electric vehicles. *Energies* **2018**, *11*, 1716. [[CrossRef](#)]
8. Kim, J.; Lee, B.; Lee, J.; Lee, S.; Park, C.; Jung, S.; Lee, S.; Yi, K.; Baek, J. Development of 1-MW inductive power transfer system for a high-speed train. *IEEE Trans. Ind. Electron.* **2015**, *62*, 6242–6250. [[CrossRef](#)]
9. Yuan, Z.; Zhang, X.; Yang, Q.; Li, Y.; Zhang, P. Asymmetric coupling mechanism of wireless power transmission system for high-speed train. *Trans. China Electrotech. Soc.* **2017**, *32*, 18–25. (In Chinese)
10. Guidi, G.; Suul, J.; Jensen, F.; Sorfonn, I. Wireless charging for ships: High-power inductive charging for battery electric and plug-in hybrid vessels. *IEEE Electr. Mag.* **2017**, *5*, 22–32. [[CrossRef](#)]
11. Li, Y.; Lu, Q.; Zhu, Z. Unbalanced magnetic force prediction in permanent magnet machines with rotor eccentricity by improved superposition method. *IET Electr. Power Appl.* **2017**, *11*, 1095–1104. [[CrossRef](#)]
12. Yamada, T.; Fujisaki, K. Basic characteristic of electromagnetic force in induction heating application of linear induction motor. *IEEE Trans. Magn.* **2008**, *44*, 4070–4073. [[CrossRef](#)]
13. Kim, D.; Park, J.; Kim, K.; Ho Park, H.; Ahn, S. Propulsion and Control of Implantable Micro-Robot Based on Wireless Power Transfer. In Proceedings of the 2015 IEEE Wireless Power Transfer Conference (WPTC), Boulder, CO, USA, 13–15 May 2015.
14. Kim, D.; Kim, M.; Yoo, J.; Ho Park, H.; Ahn, S. Magnetic resonant wireless power transfer for propulsion of implantable micro-robot. *J. Appl. Phys.* **2015**, *117*. [[CrossRef](#)]
15. Hu, J.; Liu, D.; Liao, Q.; Yan, Y.; Liang, S. Electromagnetic vibration noise analysis of transformer windings and core. *IET Electr. Power Appl.* **2016**, *10*, 251–257.
16. Jang, I.S.; Ham, S.H.; Kim, W.H.; Jin, C.S.; Cho, C.S.; Lee, K.D.; Lee, J.J.; Kang, D.; Lee, J. Method for analyzing vibrations due to electromagnetic force in electric motors. *IEEE Trans. Magn.* **2014**, *50*, 297–300. [[CrossRef](#)]
17. Lin, F.; Zuo, S.; Deng, W.; Wu, S. Modeling and analysis of electromagnetic force, vibration, and noise in permanent-magnet synchronous motor considering current harmonics. *IEEE Trans. Ind. Electron.* **2016**, *63*, 7455–7466. [[CrossRef](#)]
18. Zhang, X.; Yuan, Z.; Yang, Q.; Meng, H.; Jin, Y.; Wang, Z.; Jiang, S. High-Frequency Electromagnetic Force Characteristics on Electromagnetic Shielding Materials in Wireless Power Transmission System. In Proceedings of the 2017 IEEE PELS Workshop on Emerging Technologies: Wireless Power Transfer (WoW), Chongqing, China, 20–22 May 2017.
19. Zhang, X.; Zhang, P.; Yang, Q.; Yuan, Z.; Su, H. Magnetic shielding design and analysis for wireless charging coupler of electric vehicles based on finite element method. *Trans. China Electrotech. Soc.* **2016**, *31*, 71–79. (In Chinese) [[CrossRef](#)]

